J Mol Model (2017) 23: 180
DOI 10.1007/s00894-017-3352-6

ORIGINAL PAPER

Stability and electronic properties of praseodymium-doped silicon clusters PrSin (n = 12–21)

Yutong Feng[1] · **Jucai Yang**[1]

Received: 1 August 2016 / Accepted: 19 April 2017 / Published online: 8 May 2017
© Springer-Verlag Berlin Heidelberg 2017

Abstract The neutral $PrSi_n$ (n = 12–21) species considering various spin configurations were systematically studied using PBE0 and B3LYP schemes in combination with relativistic small-core potentials (ECP28MWB) for Pr atoms and cc-pVTZ basis set for Si atoms. The total energy, growth-pattern, equilibrium geometry, relative stability, hardness, charge transfer, and magnetic moments are calculated and discussed. The results reveal that when $n < 20$, the ground-state structure of $PrSi_n$ evaluated to be prolate clusters. Starting from $n = 20$, the ground-state structures of $PrSi_n$ are evaluated to be endohedral cagelike clusters. Although the relative stabilities based on various binding energies and different functional is different from each other, the consensus is that the $PrSi_{13}$, $PrSi_{16}$, $PrSi_{18}$, and $PrSi_{20}$ are more stable than the others, especially the $PrSi_{20}$. Analyses of hardness show that introducing Pr into Si_n (n = 12–21) elevates the photochemical sensitivity, especially for $PrSi_{20}$. Calculated result of magnetic moment and charge transfer shows that the 4*f* electrons of Pr in the clusters are changed, especially in endohedral structures such as $PrSi_{20}$, in which one electron transfers from 4*f* to 5*d* orbital. That is, the 4*f* electron of Pr in the clusters participates in bonding. The way to participate in bonding is that a 4*f* electron transfers to 5*d* orbital. Although the 4*f* electron of Pr atom participates in bonding, the total magnetic moment of $PrSi_n$ is equal to that of isolated Pr atom. The charge always transfers from Pr atom to Si_n cluster for the ground state structures of $PrSi_n$ (n = 12–19), but charge transfer is reverse for $n \geq 20$. The largest charge transfer for endohedral structure reveals that the bonding between Pr and Si_n is ionic in nature and very strong. The fullerenelike structure of $PrSi_{20}$ is the most stable among all of these clusters and can act as the building blocks for novel functional nanotubes.

Keywords $PrSi_n$ · The ground state structure · Relative stability · Magnetic moment · Charge transfer

✉ Jucai Yang
yangjc@imut.edu.cn

[1] School of Energy and Power Engineering, Inner Mongolia University of Technology, and Inner Mongolia Key Laboratory of Theoretical and Computational Chemistry Simulation, Hohhot 010051, People's Republic of China

Introduction

In recent years, considerable experimentally and theoretically studies of the metal-doped silicon clusters reported in the literature leave no doubt for their potential important application in nanotechnology and microelectronic industry, which in part is due to their enhanced stabilities and tunable electronic properties by altering composition and shape [1–6]. Especially, introducing lanthanide (Ln) atoms into a Si_n cluster was regarded as a promising approach to create cluster with new magnetic properties. Since the 4*f* electron of some of Ln atoms hardly participates in bonding, the atomic magnetic moments of Ln atom in $LnSi_n$ clusters (for example, $SmSi_n$ and $EuSi_n$) can be retained. In addition, portions of the 4*f* electron of Ln atoms are also involved in bonding. The way it can participate in bonding is that a 4*f* electron of Ln atom is transferred to 5*d* orbital, and then the 5*d* electron is involved in bonding. However, the magnetic moment is unchanged (for example $PrSi_n$ clusters in this paper), but for late rare earth metal atoms, the total magnetic moment may increase after a 4*f* electron moved to 5*d*. In this regard, Ln atoms are different from those of transition metal (TM), the magnetic moment for the latter can be quenched [7–9]. In addition, Ln-doped silicon clusters can possess excellently optical and catalytic properties. For

instance, a silicon-based optical source can be produced by introducing Er atom into silicon microcrystals [10].

Up to now, many efforts have been focused on Ln-doping Si_n clusters. The geometric and electronic structures of $LuSi_n^-$, $HoSi_n^-$, $TbSi_n^-$ ($6 \le n \le 20$) were experimentally studied by Nakajima and co-workers [4, 5]. The results suggested that Tb atom is encapsulated into the Si_n cage at $n \ge 10$, and the Ho encapsulation is still incomplete when the size of the Si cage swells to 16 atoms. Bowen et al. [6] probed into the structures and properties of $LnSi_n^-$ ($3 \le n \le 13$; Ln = Ho, Gd, Pr, Sm, Eu, Yb) by means of photoelectron spectroscopy (PES). Based on their appearance, the spectra of Eu and Yb fall into category "A", the spectra of Gd, Ho, and Pr species fall into category "B", and the spectra of Sm belong to category "AB". Our previous studies [24–26] show that, however, it is more reasonable for Ln-doped silicon systems to be divided into two groups. Specifically, the group A in which 4*f* electron of Ln atoms hardly participates in bonding contains $LnSi_n^-$ (Ln = Eu, Yb, Sm). Group B in which 4*f* electron of Ln atoms is involved in bonding contains $LnSi_n^-$ (Ln = Ho, Gd, Pr).

On the theoretical level, many computational investigations on the structures and properties have been performed for $LnSi_n$ (Ln = Lu, Yb, Ho, Gd, Eu, Sm, and La, $n < 21$) by means of density functional theory (DFT), which can provide an interesting example for evaluating the accuracies of various DFT methods [11–22]. In addition, the fullerene-like neutral species $M@Si_{20}$ (M = La, Ac, Sm, Gd, Tm, Ce, Pa, Pu, Th, Np, Pm) and their anions were studied using the ab initio projected augmented wave method. The results showed that significant magnetic moments in the most stable geometries of $PaSi_{20}$, $SmSi_{20}$, $PuSi_{20}$, $TmSi_{20}$, and $GdSi_{20}^-$ can be retained [23]. Recently, we studied not only the structures and electron affinities of $LnSi_n$ (Ln = Eu, Yb, Sm, $n < 11$) and their anions, but also the structures, stabilities, and electronic properties of $HoSi_n$ (n = 12–20) using several DFT methods [11, 24–26]. The theoretical adiabatic electron affinities evaluated by these schemes can be in excellent agreement with the experimental values.

The objectives of this work are to apply two carefully selected DFT schemes and relativistic small-core potentials (ECP) basis set for Pr atom to the determination of the total energies, growth-pattern, equilibrium geometries, relative stability, hardness, magnetic moments, and charge-transfer of the medium-sized praseodymium-doped silicon clusters $PrSi_n$ (n = 12–21) to understand their novel size-dependent electronic properties and the critical size of the Pr encapsulated into the Si frame, which can provide a guide for this type of cluster-assembled material. In consideration of the possible functional dependence of the predicted lowest-energy structures, two different functionals are selected in this work. The reason to use small-core ECP is that the 4*f* electron can participate in bonding as described above.

Computational details

The two different density functional forms used here are the B3LYP [27, 28] and PBE0 [29] functionals. The cc-pVTZ [30] is employed for Si atoms. The (14*s*13*p*10*d*8*f*6*g*)/[10*s*8*p*5*d*4*f*3*g*] segmented (SEG) basis sets and relativistic small-core effective potentials (ECP28MWB) [31] are selected for praseodymium (named as SEG/ECP). For clusters of $PrSi_n$ (n = 12–21), the stationary point of these geometries are examined by the evaluation of their harmonic vibrational frequencies to insure the optimized structures as local minima. Adopted cc-pVTZ and SEG/ECP basis sets are reasonable because the structural parameters optimized with them are nearly equal to those optimized with aug-cc-pVTZ and aug-SEG/ECP basis sets for $LnSi_n$ compounds [25]. All of the calculations were carried out using the Gaussian 09 software package [32].

When determining the most stable structures, a well-known problem is possibly missing the lowest energy isomers. For small sizes, an extensive search such as using a global optimization technique can be adopted to dispose of this problem. However, it is more and more difficult with increasing of the cluster sizes because of the much increased number of low-lying isomers, and the requiring of both an efficient optimization scheme and exact potential functions cannot be done for larger size clusters. Fortunately, based on the previous experience [11, 24–26, 33], the ground state exohedral structures of neutral $LnSi_n$ clusters can be regarded as a substitution of Ln for a Si in the most stable structure of Si_{n+1}. Therefore, two families of initial geometries are considered in the optimization process. One is exohedral isomers, namely, prolate structures generated by substitution of Pr for a Si in the most stable structure of Si_{n+1}; and another is near-spherical structures generated via constrained search based on the fullerene cage motifs. To search for the ground-state structure of $PrSi_n$ clusters the possible ground-state structure of Si_n (n = 13–21) reported previously [34–38] has been considered when constructing prolate structures of $PrSi_n$ (n = 12–20). Specifically, the tricapped-trigonal-prism (TTP) motif and the six/six (six-fold-puckered hexagonal ring Si_6 plus six-atom tetragonal bipyramid Si_6, SS) motif [37, 38] of prolate structures are selected. In addition, the spin multiplicities of doublet, quartet, and sextuplet were taken into account, and the results reveal that the most stable structures of $PrSi_n$ (n = 12–20) are quartet.

Results and discussion

Lowest-energy structures and isomers

The geometries optimized with the PBE0 and B3LYP methods for $PrSi_n$ (n = 12–21) are displayed in Fig. 1. The

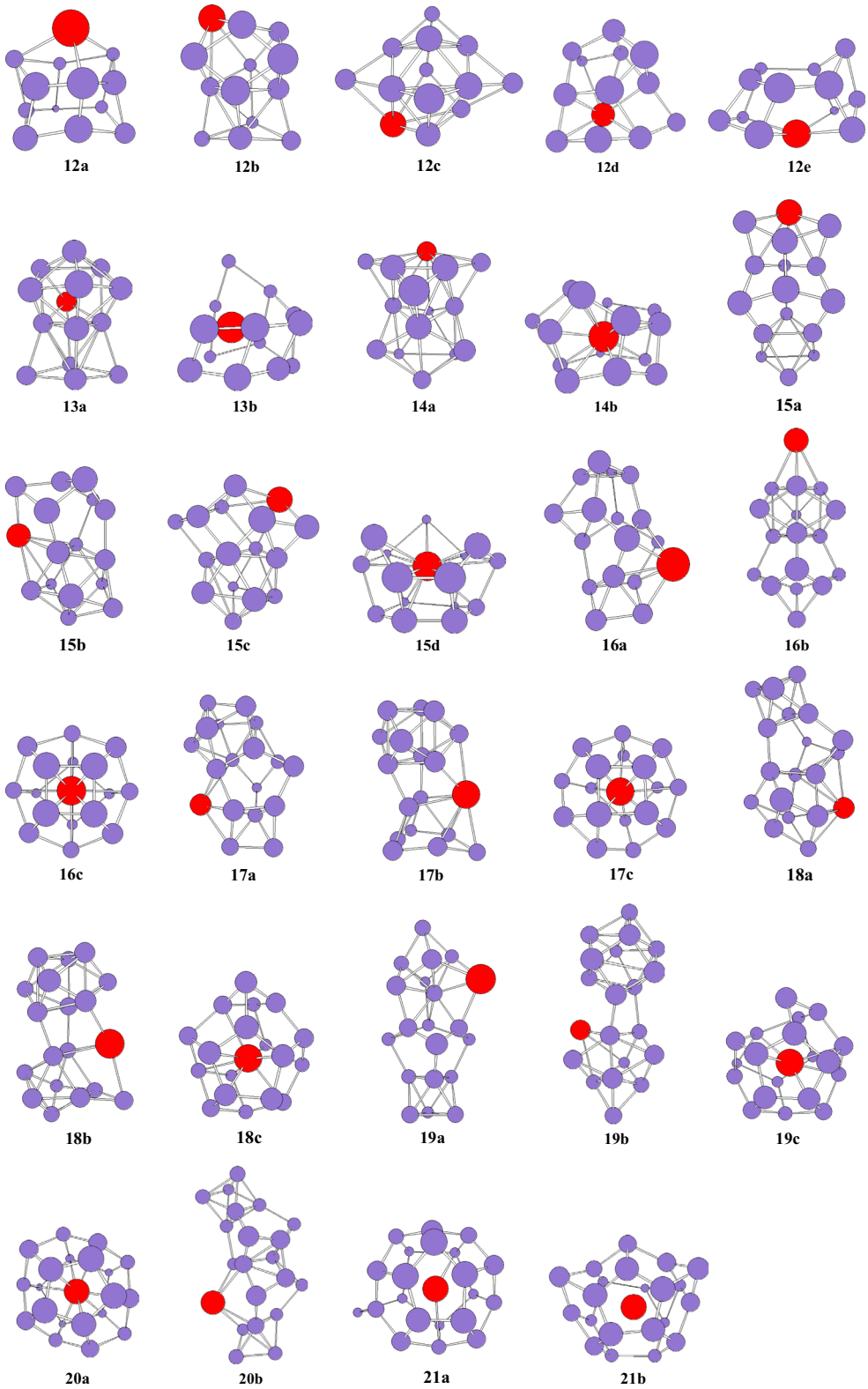

Fig. 1 The stable geometries of $PrSi_n$ (n = 12–21)

calculated total energies and relatively energy of the low-lying isomers are summarized in Table 1.

For $PrSi_{12}$, three low-lying structures are reported. Zhu et al. [34] found that the most stable structure of Si_{13} is a distorted TTP with an extra rhombus capped on one edge of the prism at the MP2 level. At quantum Monte Carlo level and MP2/aug-cc-pVTZ//B3LYP/6–31+G(d) level, the most stable structure of Si_{13} is predicted to be a trigonal antiprism with

Table 1 The point group (PG), total energy (Hartree), relative energy (ΔE, eV), spin (S), and S^2 operator for $PrSi_n$ (n = 12–21) clusters calculated with the B3LYP and the PBE0 methods

Isomer	PG	S	B3LYP			PBE0		
			S^2	Total energies	ΔE	S^2	Total energies	ΔE
12a	C_1	3/2	3.76	−3991.27685	0.00	3.76	−3989.61624	0.17
12b	C_1	3/2	3.78	−3991.26172	0.41	3.79	−3989.62252	0.00
12c	C_1	3/2	3.77	−3991.25448	0.61	3.78	−3989.61237	0.28
12d	C_1	3/2	3.78	−3991.23069	1.26	3.78	−3989.56981	1.43
12e	C_s	3/2	3.78	−3991.22966	1.28	3.78	−3989.55806	1.75
13a	C_s	3/2	3.76	−4280.79779	0.00	3.76	−4279.02838	0.00
13b	C_1	3/2	3.78	−4280.73456	1.72	3.78	−4278.93265	2.60
14a	C_s	3/2	3.76	−4570.30828	0.00	3.79	−4568.41568	0.00
14b	C_1	3/2	3.78	−4570.25495	1.45	3.86	−4568.27955	3.70
15a	C_1	3/2	3.89	−4859.84381	0.00	3.79	−4857.81319	0.00
15b	C_1	3/2	3.77	−4859.83455	0.25	3.77	−4857.80529	0.21
15c	C_1	3/2	3.75	−4859.81855	0.69	3.78	−4857.79764	0.42
15d	C_1	3/2	3.79	−4859.77643	1.83	3.80	−4857.72709	2.34
16a	C_1	3/2	3.76	−5149.37004	0.00	3.77	−5147.20972	0.00
16b	C_{3v}	3/2	3.76	−5149.35594	0.38	3.76	−5147.20452	0.14
16c	C_s	3/2	3.80	−5149.30215	1.85	3.83	−5147.15452	1.50
17a	C_1	3/2	3.76	−5438.88077	0.00	3.76	−5436.60399	0.15
17b	C_1	3/2	3.78	−5438.87549	0.14	3.78	−5436.60932	0.00
17c	C_1	3/2	3.79	−5438.83350	1.29	3.79	−5436.54596	1.72
18a	C_1	3/2	3.76	−5728.41683	0.00	3.76	−5726.00618	0.00
18b	C_1	3/2	3.78	−5728.38767	0.79	3.79	−5725.99722	0.24
18c	C_1	3/2	3.78	−5728.39715	0.54	3.80	−5725.98551	0.56
19a	C_s	3/2	3.76	−6017.93378	0.00	3.76	−6015.20823	0.00
19b	C_1	3/2	3.76	−6017.93090	0.08	3.76	−6015.20654	0.05
19c	C_1	3/2	3.78	−6017.92257	0.31	3.79	−6015.20041	0.21
20a	C_{2h}	3/2	3.78	−6307.49656	0.00	3.80	−6304.81882	0.00
20b	C_1	3/2	3.75	−6307.47576	0.57	3.76	−6304.80333	0.42
21a	C_1	3/2	3.79	−6597.00945	0.00	3.80	−6594.20502	0.00
21b	C_1	3/2	3.70	−6596.98049	0.79	3.78	−6594.19256	0.34

C_{3v}-symmetry [35] and a C_{2v}-symmetry geometry [36], respectively. The isomers **12a**, **12b**, and **12c** shown in Fig. 1 can be regarded as a substitution of Pr for a Si of three of these Si_{13} geometries. The isomers **12d** and **12e** can be obtained when placing the Pr atom inside the icosahedron and hexagonal prism of Si_{12} serve as the initio optimized geometries and undergo Jahn-Teller distortion if vibrational analysis yields one or more imaginary frequencies, respectively. The geometries of **12d** and **12e** reveal that the cage-like structure of $PrSi_{12}$ is less stable. Energetically, if the B3LYP functional is selected, the **12a** is the most stable structure, which is 0.41 eV lower than the **12b**, whereas if the PBE0 functional is selected, the **12b** is more stable than the **12a** by 0.17 eV.

For $PrSi_{13}$, two isomers are presented. The lowest-energy structure **13a** can be viewed as a substitution of Pr atom for a Si atom in the most stable structure of Si_{14} [34], a faced-capped distorted TTP with an extra rhombus capped on the prism's edge, by a substitution Pr for a Si atom. The isomer **13b** can be generated after a Si atom is added onto the Pr-encapsulated hexagonal prism of Si_{12}. It is higher than that of **13a** by 1.72 and 2.60 eV in energy at the B3LYP and PBE0 levels, respectively.

Two isomers are reported for $PrSi_{14}$. The most stable structure **14a** can be regarded as a substitution of Pr for a Si of the ground state structure of Si_{15} (a TTP with a tricapped trigonal antiprism) [34] with a Pr atom. It is more stable in energy than the cage-like **14b** isomer by 1.45 and 3.70 eV at the B3LYP and PBE0 levels, respectively.

Four isomers are presented for $PrSi_{15}$. Three structures, which contain respectively TTP, SS, and two fused pentagonal prisms, compete with each other for the most stable structure of Si_{16} [37]. The isomers **15a**, **15b**, and **15c** can be regarded as replacing a Si atom of these isomers with a Pr atom, respectively. The isomer **15d** is generated after one silicon atom is

removed from the Pr-encapsulated fullerenelike geometry of Si_{16}. Energetically, it is less stable than the **15a** by 1.83 and 2.34 eV with the B3LYP and PBE0 schemes, respectively.

For $PrSi_{16}$, two prolate and one fullerenelike structure are presented. The most stable **16a** containing SS motif is generated by replacing a Si atom of the most stable structure of Si_{17} [37]. The isomer **16b** containing TTP motif can be regarded as replacing a Si atom of Si_{17} [37]. Energetically, the prolate **16a** is more stable than the prolate **16b** and fullerenelike **16c** by 0.14 (PBE0) and 0.38 eV (B3LYP), and 1.50 (PBE0) and 1.85 eV (B3LYP), respectively.

Three isomers are presented for $PrSi_{17}$. For Si_{18}, both structures containing SS and TTP motif compete the most stable structure with each other [37]. The prolate **17a** and **17b** are obtained by replacing a Si atom of the two Si_{18} isomers with a Pr atom, respectively. The isomer **17c** is generated after one silicon atom is added to $PrSi_{16}$ of fullerenelike **16c**. Energetically, if the B3LYP functional is selected, the **17a** is the stable structure, which is more stable than the **17b** by 0.14 eV, whereas if the PBE0 functional is selected, the **17b** is more stable than the **17a** by 0.15 eV. That is, the predicted lowest-energy structure of $PrSi_{17}$, analogous to Si_{18} [37], can be dependent on the functional selected.

For $PrSi_{18}$, two prolate and one cage-like structure are presented. The most stable **18a** is generated by replacing a Si atom of the most stable structure of Si_{19} containing SS [37]. The isomer **18b** can be regarded as supplanting a Si atom of Si_{19} containing TTP motif [37]. The cage-like **18c** is generated after a Si atom is added to $PrSi_{17}$ of the cake-like **17c**. Energetically, the cake-like **18c** is less stable than the prolate **18a** by 0.56 and 0.54 eV at the PBE0 and B3LYP levels, respectively, but it is more stable than the **18b** by about 0.25 eV at the B3LYP level.

For $PrSi_{19}$, two prolate and one cage-like structure are also reported. The prolate **19a** and **19b** is regarded as supplanting a Si atom of both Si_{20} containing SS and TTP motif [37], respectively. The cage-like **19c** is generated after a Si atom is removed from the Pr-encapsulated fullerenelike structure of Si_{20}. Energetically, the **19a** structure is more stable than those of **19b** and **19c** by 0.08 and 0.31 eV at the B3LYP level, and by 0.05 and 0.21 eV at the PBE0 level, respectively.

For $PrSi_{20}$, two isomers are presented. Isomer **20b** is regarded as supplanting a Si atom of the most stable structure of Si_{21} containing SS motif [38]. Energetically, it is less stable than the fullerenelike **20a** by 0.42 and 0.57 eV with the PBE0 and B3LYP schemes, respectively.

For $PrSi_{21}$, two cagelike structures are presented. Isomer **21a** which is regarded as adding a Si atom onto the fullerenelike 2**0a** is predicted to be the ground state structure.

From the above described, we can find that the most stable structure of $PrSi_n$, starting from $n = 20$, are predicted to be endohedral cagelike species. When $n < 20$, the ground-state structures of $PrSi_n$ are prolate clusters, which can be generated by a substitution of Pr for a Si atom of the most stable structures of Si_{n+1}. The ground-state structures of $PrSi_n$ are favorable to contain SS motif when $n = 16$–19, while when $n < 16$, the ground-state structures of $PrSi_n$ are favorable to contain TTP motif.

Binding energies

To probe the inherent stabilities of most stable $PrSi_n$ ($n = 12$–21) clusters, the binding energies per atom (BEPA) (defined as the required energy in the reaction $PrSi_n \rightarrow Pr + nSi$, namely, $BEPA(PrSi_n) = [nE(Si) + E(Pr)-E(PrSi_n)]/(n + 1)$) of $PrSi_n$ are predicted using the PBE0 and B3LYP methods. A plot of the BEPA against the corresponding cluster size shown in Fig. 2 indicates that at the B3LYP level, $PrSi_{13}$, $PrSi_{16}$, $PrSi_{18}$, and $PrSi_{20}$ are slightly more stable than the others because they correspond to the four "bumps" of curve, respectively. While at the PBE0 level, $PrSi_{13}$, $PrSi_{16}$, and $PrSi_{20}$ are slightly more stable suggested by the smoothly increasing background.

In additional to the BEPA, the dissociation energies are also illustrated in order to compare the stabilities of various $PrSi_n$ species. The dissociation energies are shown in Fig. 3 (defined as the required energies for the disproportionation reaction $2PrSi_n \rightarrow PrSi_{n+1} + PrSi_{n-1}$, namely, $DE1(PrSi_n) = [E(PrSi_{n+1}) + E(PrSi_{n-1})-2E(PrSi_n)]$). This gives a sensitive measure of relative stability. As can be seen from Fig. 3, three local minimal values with $n = 14$, 17, and 19 are found, reflecting that $PrSi_{14}$, $PrSi_{17}$, and $PrSi_{19}$ have weaker local stabilities when compared with the others at the B3LYP and PBE0 levels.

Another measure of the stability is given by the dissociation energies, $DE2(PrSi_n) = [E(Si_n) + E(Pr) - E(PrSi_n)]$, $DE3(PrSi_n) = [E(PrSi_{n-1}) + E(Si) - E(PrSi_n)]$, and $DE4(Si_n) = [E(Si_{n-1}) + E(Si) - E(Si_n)]$, respectively. They are plotted in Figs. 4 and 5. From Fig. 4 we can see that at the B3LYP level, the $PrSi_n$ for $n = 13$, 16, 18, and 20 are more stable than the others because their DE2 are local maximal values. On the other hand, the analysis of DE3 and DE4 reveals that the $PrSi_n$ for $n = 13$, 15, 16, 18, and 20 are more stable than the others in respect that the DE3 is larger than the DE4. In other words, when an extra Si atom is attached to the cluster, it is energetically more favorable to add to $PrSi_{n-1}$ and to form $PrSi_n$ species rather than to add to Si_{n-1} cluster and to form Si_n cluster. From Fig. 5 we can conclude that using the PBE0 scheme, the result of analysis of DE2 is the same as that of analysis of DE3 and DE4. That is, the $PrSi_n$ for $n = 13$, 16, and 20 are more stable than the others in respect that the DE2 are local maximal values.

Although the relative stabilities based on various binding energies and different functional is different from each other, the consensus is that the $PrSi_{13}$, $PrSi_{16}$, and $PrSi_{20}$ are more stable than the others, especially the $PrSi_{20}$, of which various binding energies are obviously larger than those of $PrSi_{13}$ and

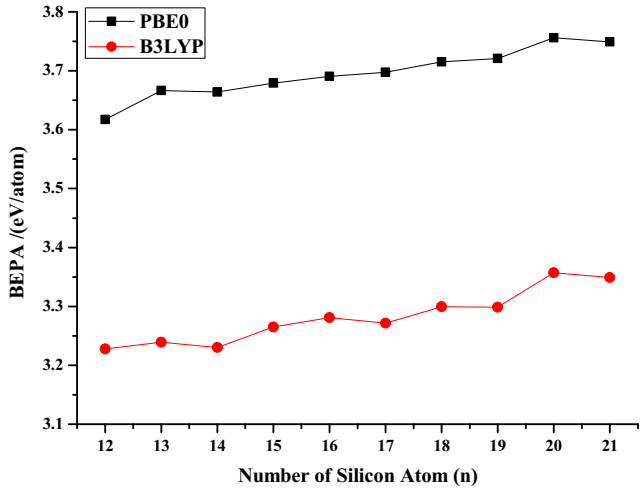

Fig. 2 The binding energies per atom (BEPA) for the most stable $PrSi_n$ (n = 12–21) clusters calculated with the PBE0 and the B3LYP methods

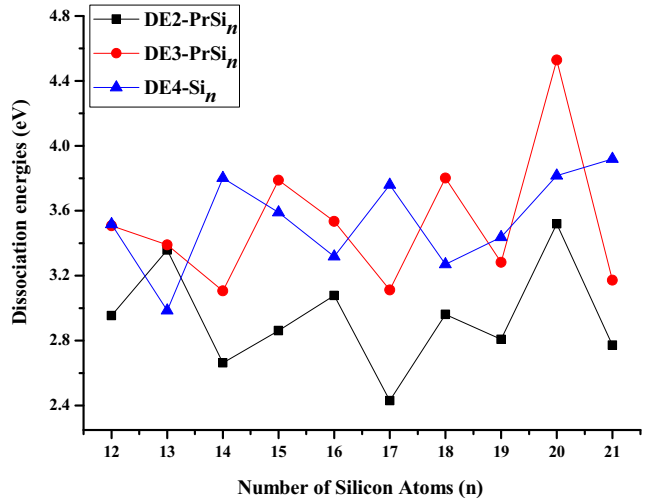

Fig. 4 DE2, DE3, and DE4 (eV) of $PrSi_n$ (n = 12–21) versus the number of atoms n calculated with the B3LYP method

$PrSi_{16}$. It is noticed that $PrSi_{20}$ structures can act as the building blocks for nanotubes due to their cage-like geometry.

Hardness

In a sense, hardness is not only an important physical property, but also a significant criterion to mirror the chemical reactivity of species, especially for Ln-doped Si clusters which always have good photochemical sensitivity. The hardness (which is defined as the difference between the energy of the HOMO and the LUMO) for the most stable structures of $PrSi_n$ (n = 12–21) clusters predicted by the two methods are plotted in Fig. 6. The hardness of Si_n species for comparison is also sketched in Fig. 6. From Fig. 6 we can conclude that (1) the hardness curves of the B3LYP and the PBE0 are on the whole in parallel, and the hardness of the PBE0 is larger than that of B3LYP. The reason is that the HOMO energies and the LUMO energies predicted in Kohn-Sham (KS) molecular orbital model undergo approximately the same amount of upshift, while Hartree-Fock (HF) hybrids shift the LUMO up to much higher energy levels than the HOMO up [39]. On the other hand, the component of HF hybrid in the PBE0 is larger than that in the B3LYP. So the HOMO-LUMO gap of the PBE0 is larger than that of the B3LYP. The KS HOMO-LUMO gap in molecules approximates the lowest excitation energy much more closely than the HF HOMO-LUMO gap does [39]. So the B3LYP HOMO-LUMO gap may be a better approximation to the optical gap in molecules than the PBE0 HOMO-LUMO gap. (2) The hardness of $PrSi_n$ is smaller than that of pure Si_n clusters. This shows that introducing Pr atom into Si_n clusters elevates the photochemical sensitivity. (3) The smaller the hardness, the easier the $PrSi_n$ inclines to ignite the photochemical reaction. The hardness of $PrSi_{16}$, $PrSi_{17}$, $PrSi_{18}$, $PrSi_{20}$, and $PrSi_{21}$ is smaller than the others, namely, their photochemical sensitivity is better than the others.

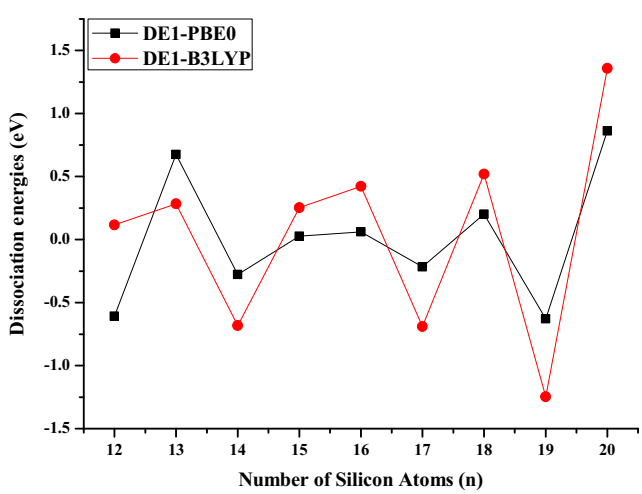

Fig. 3 DE1 (eV) of $PrSi_n$ (n = 12–20) versus the number of atoms n

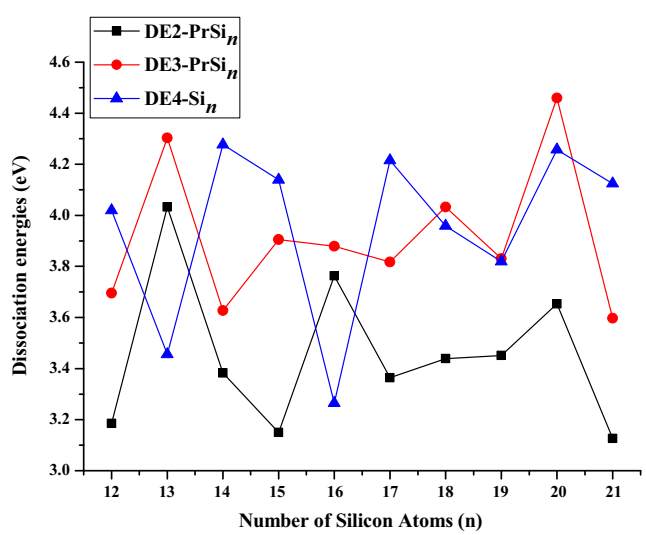

Fig. 5 DE2, DE3, and DE4 (eV) of $PrSi_n$ (n = 12–21) versus the number of atoms n calculated with the PBE0 method

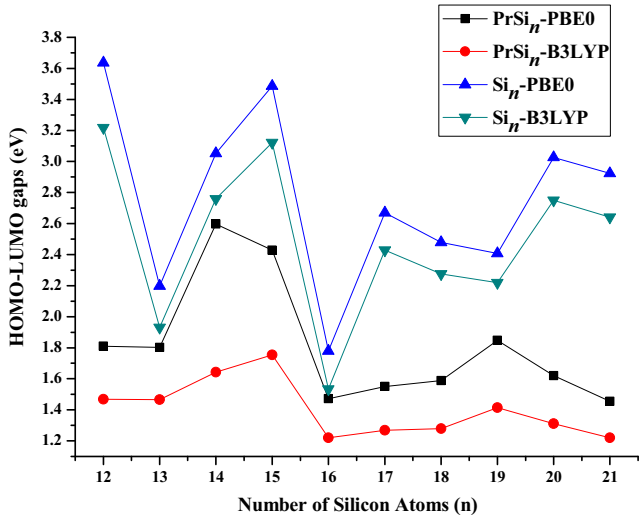

Fig. 6 The HOMO-LUMO gaps of $PrSi_n$ and Si_n (n = 12–21) calculated with the PBE0 and the B3LYP methods

Magnetic moment and charge transfer

To better understand the interaction between the Pr atom and silicon clusters, natural population analyses (NPA) are carried out with the two schemes. The analyses of charge and NPA valence configurations of Pr atom listed in Table 2 reveal that (1) the valence configurations are $6s^{0.12–0.31}4f^{2.17–2.89}5d^{0.90–1.91}6p^{0.09–0.33}$ and $6s^{0.13–0.38}4f^{2.36–2.90}5d^{0.82–1.42}6p^{0.07–0.29}$ for Pr in $PrSi_n$ (n = 12–19) species at the PBE0 and the B3LYP levels, and $6s^{0.37}4f^{2.03–2.07}5d^{4.52–4.53}6p^{1.53–1.55}$ and $6s^{0.33–0.34}4f^{2.05–2.06}5d^{4.03–4.16}6p^{1.41–1.44}$ for Pr in $PrSi_{20}$ and $PrSi_{21}$, respectively. Evidently, in the clusters the 4*f* electron of Pr is changed, especially in cagelike structures such as $PrSi_{20}$ and $PrSi_{20}$, in which one electron transfers from 4*f* to 5*d* orbital (the configuration of isolated Pr atom is $[core]6s^2 4f^3 5d^0 6p^0$). In this regard, Pr atom differs from Eu and Sm. The 4*f* shell of those in the clusters has almost no change [24, 25]. Apart from the charge transfer from 4*f* to 5*d* orbital, charge transfer takes place from 6*s* to 5*d* orbital, thus, resulting in hybridization between 6*s* and 5*d* orbital. (2) The charge always transfers from Pr atom to Si_n cluster for $PrSi_n$ (n = 12–19), but charge transfer is reversed for $PrSi_{20}$ and $PrSi_{22}$, which reveals that Pr atom acts as an electron acceptor in the cage-like ground-state structure. The transferred charges are largest (2.99–3.49*e*) for $PrSi_{20}$, which reveals that the bonding between Pr atom and Si_n cluster is ionic in nature, and the strong bonding results in the most stable cage-like structure of $PrSi_{20}$ among all of these species studied in this work. This result is in agreement with that of DE analyses.

Table 2 Natural population analysis (NPA) valence configurations and charge of Pr atom (in a.u.) calculated with the B3LYP and the PBE0 methods for the lowest energy $PrSi_n$ (n = 12–21) species

Isomer	Method	Electron configuration	Charge
12a	B3LYP	$[core]6S^{0.13}4f^{2.85}5d^{1.03}6p^{0.17}$	0.87
	PBE0	$[core]6S^{0.13}4f^{2.82}5d^{1.12}6p^{0.19}$	0.80
13a	B3LYP	$[core]6S^{0.17}4f^{2.83}5d^{1.02}6p^{0.12}$	0.92
	PBE0	$[core]6S^{0.15}4f^{2.81}5d^{1.08}6p^{0.14}$	0.88
14a	B3LYP	$[core]6S^{0.23}4f^{2.46}5d^{1.42}6p^{0.24}$	0.70
	PBE0	$[core]6S^{0.24}4f^{2.17}5d^{1.91}6p^{0.33}$	0.40
15a	B3LYP	$[core]6S^{0.38}4f^{2.36}5d^{1.41}6p^{0.29}$	0.72
	PBE0	$[core]6S^{0.31}4f^{2.18}5d^{1.81}6p^{0.25}$	0.52
16a	B3LYP	$[core]6S^{0.19}4f^{2.72}5d^{1.18}6p^{0.18}$	0.80
	PBE0	$[core]6S^{0.18}4f^{2.59}5d^{1.44}6p^{0.22}$	0.63
17a	B3LYP	$[core]6S^{0.13}4f^{2.90}5d^{0.82}6p^{0.15}$	1.04
	PBE0	$[core]6S^{0.13}4f^{2.89}5d^{0.90}6p^{0.17}$	0.96
18a	B3LYP	$[core]6S^{0.17}4f^{2.86}5d^{0.95}6p^{0.16}$	0.91
	PBE0	$[core]6S^{0.16}4f^{2.86}5d^{1.01}6p^{0.17}$	0.85
19a	B3LYP	$[core]6S^{0.14}4f^{2.81}5d^{0.93}6p^{0.07}$	1.10
	PBE0	$[core]6S^{0.12}4f^{2.71}5d^{1.09}6p^{0.09}$	1.04
20a	B3LYP	$[core]6S^{0.34}4f^{2.05}5d^{4.16}6p^{1.44}$	−2.99
	PBE0	$[core]6S^{0.36}4f^{2.07}5d^{4.53}6p^{1.53}$	−3.49
21a	B3LYP	$[core]6S^{0.33}4f^{2.06}5d^{4.03}6p^{1.41}$	−2.82
	PBE0	$[core]6S^{0.36}4f^{2.03}5d^{4.52}6p^{1.55}$	−3.46

Table 3 Magnetic moment (μB) of 6*s*, 4*f*, 5*d*, 6*p* states for Pr atom, total magnetic moment (μB) of Pr atom, and total magnetic moment of the ground-state structure of $PrSi_n$ (n = 12–21) calculated with the B3LYP and the PBE0 methods

Isomer	Method	Pr magnetic moment					Molecule
		6 *s*	4*f*	5*d*	5*p*	Total	
12a	B3LYP	0.03	2.81	0.09	0.00	2.93	3
	PBE0	0.03	2.79	0.11	0.01	2.94	3
13a	B3LYP	0.01	2.79	0.10	0.00	2.90	3
	PBE0	0.01	2.78	0.12	0.00	2.91	3
14a	B3LYP	0.01	2.42	0.16	0.00	2.59	3
	PBE0	0.00	2.09	0.26	0.00	2.35	3
15a	B3LYP	0.01	2.30	0.25	0.01	2.57	3
	PBE0	0.00	2.08	0.33	0.01	2.42	3
16a	B3LYP	0.01	2.68	0.12	0.00	2.81	3
	PBE0	0.01	2.54	0.18	0.00	2.73	3
17a	B3LYP	0.00	2.88	0.06	0.00	2.94	3
	PBE0	0.01	2.86	0.08	0.00	2.95	3
18a	B3LYP	0.01	2.84	0.08	0.00	2.93	3
	PBE0	0.00	2.83	0.09	0.01	2.93	3
19a	B3LYP	0.02	2.78	0.11	0.00	2.91	3
	PBE0	0.01	2.68	0.17	0.01	2.87	3
20a	B3LYP	0.00	1.97	0.04	0.00	2.03	3
	PBE0	0.00	1.98	0.01	0.00	1.99	3
21a	B3LYP	0.00	2.00	0.04	0.01	2.05	3
	PBE0	0.00	1.95	0.08	0.00	2.03	3

Magnetic moments are one of the most interesting properties in physics. The analyses of magnetic moments listed in Table 3 show that the total magnetic moments of $PrSi_n$ (n = 12–20) are 3 μB, which is mainly from the 4*f* state (1.97–2.88 μB) of Pr atom, following this is the 5*d* state (0.01–0.33 μB), and the remaining states are 3*s* and 3*p* (0.06–1.01 μB) of Si atoms (the 6*s* and 6*p* states of Pr atom have very little contribution). This is to say that although the 4*f* electron of Pr atom participates in bonding, the total magnetic moment of $PrSi_n$ is idential to that of isolated Pr atom.

Conclusions

The total energies, growth-pattern, equilibrium geometries, relative stability, hardness, magnetic moments, and charge-transfer of $PrSi_n$ (n = 12–20) species have been investigated with the PBE0 and the B3LYP functionals in combination with the SEG/ECP basis set for the Pr atoms and cc-PVTZ basis set for the Si atoms. The results reveal that (1) when $n < 20$, the ground-state structure of $PrSi_n$ predicted to be prolate clusters, which can be generated by a substitution of Pr atom for a Si of the ground-state structures of Si_{n+1}. To be more precise, the ground-state structure of $PrSi_n$ prefers to contain SS motif when n = 16–19, while it prefers to contain TTP motif when $n < 16$. Starting from $n = 20$, the ground-state structures of $PrSi_n$ are evaluated to be endohedral cagelike clusters. (2) Although the relative stabilities based on various binding energies and different functional is different from each other, the consensus is that the $PrSi_{13}$, $PrSi_{16}$, and $PrSi_{20}$ are more stable than the others, especially the $PrSi_{20}$. (3) Analysis of hardness shows that introducing Pr atom to Si_n (n = 12–20) clusters elevates the photochemical sensitivity. (4) The natural population analysis (NPA) shows that the 4*f* electrons of Pr in the clusters are changed, especially in $PrSi_{20}$ and $PrSi_{21}$, in which one electron transfers from 4*f* to 5*d* orbital. This is to say that the 4*f* electron of Pr in the clusters participates in bonding. The way to participate in bonding is that a 4*f* electron transfers to 5*d* orbital. Although the 4*f* electron of Pr atom participates in bonding, the total magnetic moment of $PrSi_n$ is equal to that of isolated Pr atom. The charge always transfers from Pr atom to Si_n cluster for the ground state structures of $PrSi_n$ (n = 12–19), but charge transfer is reversed for $PrSi_{20}$ and $PrSi_{21}$, which reveals that Pr acts as an electron acceptor in the cage-like ground-state structure. The largest charge transfer for $PrSi_{20}$ reveals that the bonding between Pr atom and Si_n cluster is ionic in nature and very strong. As a result, the fullerenelike structure of $PrSi_{20}$ is the most stable one and can act as the building blocks for novel functional nanotubes.

Acknowledgments This study was economically supported by the National Natural Science Foundation of China (Grant No. 21263010), by the Inner Mongolia Natural Science Foundation (Grant No. 2015MS0216), and by the Program for Innovative Research Team in University of the Inner Mongolia Autonomous Region (Grant no. NMGIRT-A-1603).

References

1. Avaltroni F, Steinmann SN, Corminboeuf C (2012) Phys Chem Chem Phys 14:14842–14849
2. Tam NM, Tai TB, Ngan VT, Nguyen MT (2013) J Phys Chem A 117:6867–6882
3. Lin L, Yang JC (2015) J Mol Model 21(155):1–13
4. Ohara M, Miyajima K, Pramann A, Nakajima A, Kaya K (2002) J Chem Phys A 106:3702–3705
5. Koyasu K, Atobe J, Furuse S, Nakajima A (2008) J Chem Phys 129(214301):1–7
6. Grubisic A, Ko YJ, Wang H, Bowen KH (2009) J Am Chem Soc 131:10783–10790
7. Li JR, Wang GH, Yao CH, Mu YW, Wan JG, Han M (2009) J Chem Phys 130(164514):1–9
8. Guo LJ, Zhao GF, Gu YZ, Liu X, Zeng Z (2008) Phys Rev B 77(195417):1–8
9. Wang JG, Zhao JJ, Ma L, Wang BL, Wang GH (2007) Phys Lett A 367:335–344
10. Kenyon AJ (2005) Semicond Sci Technol 20:R65–R84
11. Hou LY, Yang JC, Liu YM (2016) J Mol Model 22(193):1–10
12. Peng Q, Shen J (2008) J. Chem. Phys. 128(084711):1–11
13. Zhao GF, Sun JM, Gu YZ, Wang YX (2009) J Chem Phys 131: 114312-1–114312-7
14. Li CG, Pan LJ, Shao P, Ding LP, Feng HT, Luo DB, Liu B (2015) Theor Chem Accounts 134(34):1–11
15. Liu TG, Zhao GF, Wang YX (2011) Phys Lett A 375:1120–1127
16. Liu TG, Zhang WQ, Li YL (2014) Front Phys 9:210–218
17. Zhao RN, Ren ZY, Guo P, Bai JT, Zhang CH, Han JG (2006) J Phys Chem A 110:4071–4079
18. Zhao RN, Han JG, Bai JT, Liu FY, Sheng LS (2010) Chem Phys 372:89–95
19. Zhao RN, Han JG, Bai JT, Sheng LS (2010) Chem Phys 378:82–87
20. Cao TT, Zhao LX, Feng XJ, Lei YM, Luo YH (2009) J Mol Struct 895:148–155
21. Wang HQ, Li HF (2014) RSC Adv 4:29782–29793
22. Zhao RN, Han JG (2014) RSC Adv 4:64410–64418
23. Kumar V, Singh AK, Kawazoe Y (2006) Phys Rev B 74(125411): 1–5
24. Yang JC, Wang J, Hao YR (2015) Theor Chem Accounts 134(81): 1–11
25. Xie XH, Hao DS, Liu YM, Yang JC (2015) Comput Theor Chem 1074:1–8
26. Xie XH, Hao DS, Yang JC (2015) Chem Phys 461:11–19
27. Becke AD (1993) J Chem Phys 98:5648–5652
28. Lee C, Yang W, Parr RG (1988) Phys Rev B 37:785–789
29. Adamo C, Barone V (1999) J Chem Phys 110:6158–6170
30. Woon DE, Dunning Jr TH (1993) J Chem Phys 98:1358–1371
31. Cao X, Dolg M (2002) J Mol Struct THEOCHEM 581:139–147
32. Frisch MJ, Trucks GW, Schlegel HB, Scuseria GE, Robb MA, Cheeseman JR, Scalmani G, Barone V, et al. (2010) Gaussian 09 revision C.01. Gaussian Inc, Wallingford
33. Yang JC, Feng YT, Xie XH, Wu HW (2016) Theor Chem Accounts 135(204):1–12

34. Zhu XL, Zeng XC, Lei YA, Pan B (2004) J Chem Phys 120:8985–8995
35. Grossman JC, Mitáš L (1995) Phys Rev Lett 74:1323–1326
36. Nigam S, Majumder C, Kulshreshtha SK (2006) J Chem Phys 125(074303):1–11
37. Yoo S, Zeng XC (2005) J Chem Phys 123(164303):1–6
38. Yoo S, Zeng XC (2006) J. Chem. Phys. 124(054304):1–6
39. Baerends EJ, Gritsenko OV, van Meer R (2013) 15:(39)16408-16425